INCORPORATING GEOLOGIC CONTEXT TO CONSTRAIN THE COMPOSITION AND MATURITY OF MERCURY'S SURFACE FROM MULTISPECTRAL IMAGING. M. A. Riner[1] and P. G. Lucey[2], [1]Planetary Science Institute, 1700 East Fort Lowell, Suite 106, Tucson, AZ, 85719, mariner@psi.edu, [2]Hawaii Institute of Geophysics and Planetology, University of Hawaii, Manoa, 1680 East-West Rd., Honolulu, HI 96822.

Introduction: The mineral composition of Mercury's surface is poorly known. Unfortunately, spectra of Mercury's surface are featureless throughout the visible to near infrared (VIS-NIR) and traditional reflectance spectroscopy techniques have faced intractable challenges to unique identification of surface mineralogy. These challenges are related to the low iron content of Mercury's surface and intense space wreathing that obscures potential absorption features, even in the least altered surface exposures. Understanding the optical effects of space weathering on Mercury will yield insights into the physical and chemical processes involved, aid comparisons to space weathering on the Moon and asteroids and aid in mitigating the optical effects of space weathering in compositional studies of Mercury's surface. Here we present the results of incorporating geologic context to the interpretation of radiative transfer modeling of VIS_NIR spectra of Mercury's surface from the MESSENGER Mercury Dual Imaging System (MDIS) instrument.

Reflectance variations on Mercury span a continuum from relatively bright materials with a steep spectral slope to dark materials with a shallower slope. Based on spectral and geologic criteria, three major crustal terrains have been identified: high reflectance smooth plains (HSP), intermediate terrain (IT), and low reflectance materials (LRM) [1]. Fig 1.

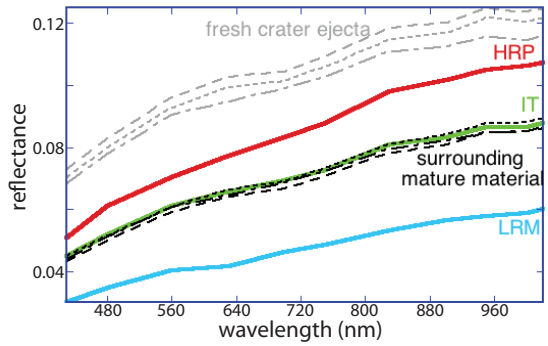

Fig. 1 – MDIS spectra of average mature high reflectance plains (HRP, red), mature intermediate terrain (IT green), mature low reflectance materials (LRM, blue), immature IT fresh crater ejecta (light gray) and mature IT material surrounding each fresh crater. The line type (dash length) matches for adjoining mature/immature spectra. Spectra are in radiance factor (reflectance) relative to an identically illuminated Lambertian surface. photometrically corrected to 30° phase angle [2].

Space weathering describes the physical and chemical changes to a surface exposed to the space environment. The physical and chemical effects of space weathering include: decrease in the particle size of a surface, formation of impact glass and agglutinates (aggregates of lithic and mineral fragments welded together by impact glass), and reduction and vapor deposition of ferrous iron to coat the surfaces of larger grains. The optical effects of space weathering include: a decrease in overall reflectance (darkening), an increase in the steepness of the positive spectral slope (reddening), and the attenuation of absorption features [3-5].

Lunar space weathering has been characterized by inspection of lunar samples [6-7]. Differences in the impactor population, impact rate, impact velocity, proximity to the Sun, surface temperature, strength and composition of the solar wind, and surface composition may affect the relative importance of the physical and chemical processes involved in space weathering and a subsequent change in the spectral changes that result [8]. Yet superficially, spectra of Mercury suggest a generally lunar-like space weathering process: Mercury is dark, red, and NIR absorption bands are either absent or subdued to the point of invisibility [9].

The optical effects of space weathering present serious challenges to remote sensing studies of Mercury. Radiative transfer modeling can tie the optical effects of space wreathing to the physical products produced by alteration and in turn shed light on the relative importance of the physical and chemical processes involved in different space environments.

Hapke [10] used Maxwell-Garnet equivalent theory to combine the optical properties of space weathering derived iron (here called SMFe – Submicroscopic Metallic Iron) and unweathered host material to successfully model the laboratory spectra of a lunar rock-soil pair. Noble and coworkers [11] measured the spectra of Fe-infused silica gel samples and found the size of iron particles controlled their spectral properties. Iron metal particles much smaller than the wavelength of light (here called npFe – nanophase iron) cause darkening and reddening of the spectrum while iron particles approaching the wavelength of light (here called Britt-Pieters particles) only darken the spectrum (Figure 1). Lucey and Noble [12] tested the Hapke [10] model against the silica gel spectra and found good agreement for iron particles approaching the wavelength of light (< 40 nm). However, larger space weathering derived iron particles do occur in lunar soils, typically associated with agglutinates.

Lucey and Riner [13] added a Mie scattering component to the Rayleigh scattering-based model of Hapke [10] to explicitly model the optical effects of Britt-Pieters particles. The model is able to produce the laboratory spectra of returned lunar samples, given the

measured chemical and mineral composition along with the abundance of npFe and Britt-Pieters particles [13-14]. The model has been applied to both MESSENGER Mercury Atmosphere and Surface Composition Spectrometer (MASCS) and MDIS spectra.

Previous Results: The model of Lucey and Riner [13] has been applied to both MESSENGER MASCS and MDIS data to reproduce the low albedo and spectral slope of Mercury from four input components:

1) bright 70% reflectance – low Fe silicates
2) dark 4% reflectance – opaque component
3) nanophase iron particles (< 50 nm diameter)
4) Britt-Pieters particles (1000 nm diameter).

There is an ambiguity in the model between the competing darkening effects of Britt-Pieters particles and the opaque component. Thus previous work was able to constrain but not uniquely determine the abundance of the four input components.

New Results: Due to the smoothly varying spectra of Mercury and the lack of clear absorption bands in the VIS-NIR, the model works well with both hyper spectral (MASCS) and multispectral (MDIS) data (Fig. 2). The higher spatial resolution and geologic context provided by MDIS images have allowed us to further constrain the abundance of bright silicate minerals, an unknown opaque component, npFe, and Britt-Pieters particles.

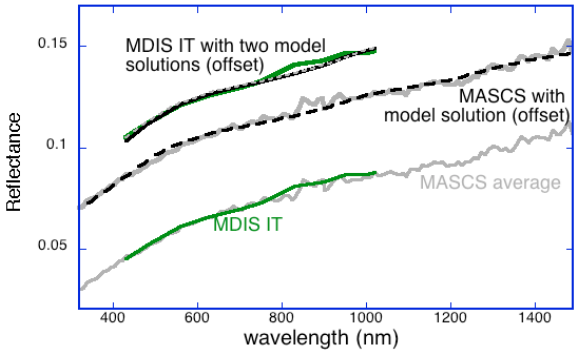

Fig. 2 – **(Bottom)** Comparison of the average of MASCS spectra obtained during flyby 1 with incidence angles less than 20 degrees (gray) with an average MDIS intermediate terrain (IT) spectrum (green). **(Middle)** MASCS observed spectrum (gray) with model fit (black), both equally offset. **(Top)** MDIS IT (green) observed with two different model fits (black and gray). Significantly different model parameters can produce equally valid spectral matches.

We have developed a constrained nonlinear optimization algorithm to select from multiple equally good spectral matches for pixels based on their geologic context. Initially, we have compiled a training catalog of small, fresh craters that have excavated optically immature (or less mature) materials within regionally uniform crustal units. The spectra of the fresh crater ejecta and the surrounding homogeneous mature crust should share the same composition and aid in isolating space weathering effects.

Initially we used a subset of 25 mature-immature spectral pairs within the intermediate terrain (IT) manually extracted from the global MDIS mosaic to develop our constrained nonlinear optimization model. For each spectra (50 in all) we identified the full range of plausible spectral matches (using the grid search method of Riner and Lucey [15]). For each mature-immature spectral pair we constrained the optimization algorithm such that each pair has the same composition (within the variation required for the sum of all four input components to equal one) but the mature spectral must have higher *total space weathering derived iron*. The relative abundance of npFe and Britt-Pieters particles is not constrained at this time. We iterate through the optimization model, adjusting the optimized solution for each spectral pair while limiting compositional variations between the 25 intermediate terrain craters.

The initial results from out constrained nonlinear optimization algorithm, applied only to intermediate terrain, mature-immature spectral pairs have further constrained the range of allowable compositions and abundance of space weathering derived products, suggesting the total space weathering derived iron for **immature** IT crater ejecta is at least 1.9 wt%, more than double the SMFe abundance in the most mature analyzed lunar samples.

Work in Progress: The addition of mature-immature spectral pairs from the LRM and HRP is underway. When the behavior of the constrained nonlinear optimization algorithm for these data is fully understood and appropriate constraints implemented we will process each set of single terrain mature-immature spectral pairs as described above. Then we will integrate the optimization of all three terrains mature-immature spectral pairs under the assumption that the composition of the terrains is:

$LRM_{opaque} > IT_{opaque} > HRP_{opaque}$

If additional constraints are necessary to derive a unique solution, we will assume that:

$LRM_{SMFe} > IT_{SMFe} > HRP_{SMFe}$

following the conclusions of Lucey and Riner [15], which demonstrated that the opaque component likely hosts the unweathered materials that are converted to SMFe by the physical and chemical processes of space weathering.

References: [1] Robinson, M.R. et al. (2008) *Sci.* 321, 66-69. [2] Domingue, D.L. et al. (2008) *Icarus* 209(1), 101-124. [3] Keller, L. and McKay, D. (1997) *GCA* 61, 2331-2340. [4] Pieters, C.M. et al. (2000) *MAPS* 35, 1101-1107. [5] Noble, S.K. et al. (2003) *Solar Sys Res*. 37(1) 31-35. [6] McCord and Adams (1973). [7] Fischer and Pieters (1994). [8] Cintala (1992). [9] Vilas, F. (1985). [10] Hapke (2000). [11] Noble, S.K. et al. (2007) *Icarus*. [12] Lucey, P.G. and Noble, S.K. (2008). [13] Lucey and Riner (2011). [14] Morris (1980). [15] Riner, M.R. and Lucey, P.G. (2012) *GRL* 39 L12201.